electronics

MDPI

Article

Ground Fault Detection of Photovoltaic and Energy Storage DC Converter Load on User Side

Kai Zhang [1,*], Jian Yang [2], Jian Li [2], Zhongying Zhang [2], Ling Gu [3] and Zhonghao Dongye [4,*]

[1] State Grid Ningjin Electric Power Supply Company, Ningjin 055550, China
[2] State Grid Xingtai Electric Power Supply Company, Xingtai 054000, China; xt_yangj2@he.sgcc.com.cn (J.Y.); xt_lij@he.sgcc.com.cn (J.L.); xt_zhangzy1@he.sgcc.com.cn (Z.Z.)
[3] Beijing NARI-EPRI Power Utilization Technology Co., Ltd., Beijing 100000, China; guling@sgepri.sgcc.com.cn
[4] State Key Laboratory of Alternate Electrical Power System with Renewable Energy Sources, North China Electric Power University, Beijing 102206, China
* Correspondence: xt_zk@he.sgcc.com.cn (K.Z.); dyzhh@ncepu.edu.cn (Z.D.)

Abstract: With the rapid development of DC power supply technology, the operation, maintenance, and fault detection of DC power supply equipment and devices on the user side have become important tasks in power load management. DC/DC converters, as core components of photovoltaic and energy storage DC systems, have issues with detecting ground faults on the positive and negative input/output buses, leading to difficulties in troubleshooting device malfunctions and potentially endangering user safety. To address these issues, a method for detecting ground faults on the positive and negative buses of a synchronous buck photovoltaic and energy storage DC/DC converter is proposed, which involves the comprehensive measurement of multi-point common-mode voltages. This method collects the input positive bus voltage, output positive bus voltage, switch voltage, and the common-mode voltage at the midpoint of the bridge arm, then sums these after removing the switching harmonics. By analyzing the characteristic differences of the summed voltage under the ground fault modes of the positive and negative input/output buses, characteristic parameters are extracted to establish a ground fault identification method, thereby achieving effective detection of ground faults in the photovoltaic and energy storage DC/DC converter. Finally, the effectiveness of the method proposed in this paper was validated through simulations and experiments.

Keywords: load management; buck converter; ground fault; fault detection

Citation: Zhang, K.; Yang, J.; Li, J.; Zhang, Z.; Gu, L.; Dongye, Z. Ground Fault Detection of Photovoltaic and Energy Storage DC Converter Load on User Side. *Electronics* **2024**, *13*, 4505. https://doi.org/10.3390/electronics13224505

Academic Editor: Ahmed Abu-Siada

Received: 14 October 2024
Revised: 10 November 2024
Accepted: 13 November 2024
Published: 16 November 2024

1. Introduction

At present, under the dual carbon goal, the construction of China's new power system is advancing rapidly. With the increasing share of distributed photovoltaic and storage systems on the load side, the operational management of new power loads urgently needs to be addressed. As a critical part of load-side operations and maintenance management, distributed photovoltaic and storage DC devices play a significant role in research related to user-side terminals and on-site detection. As shown in Figure 1, the new power load management system includes power quality monitoring, electricity billing management, load management, database management systems, safety management systems, smart energy units, data acquisition modules, and more. This system can realize real-time monitoring of terminal power load resources, collect data on power consumption and power quality over different time periods, and generate load curves and power quality reports, providing data support for load forecasting. As a key energy conversion device, the reliability of the DC/DC converter has become a significant research focus [1–3]. If a grounding fault occurs in a DC/DC converter and is not promptly addressed, it can cause the equipment to malfunction. Therefore, quickly identifying grounding faults and accurately locating the fault position has become increasingly important.

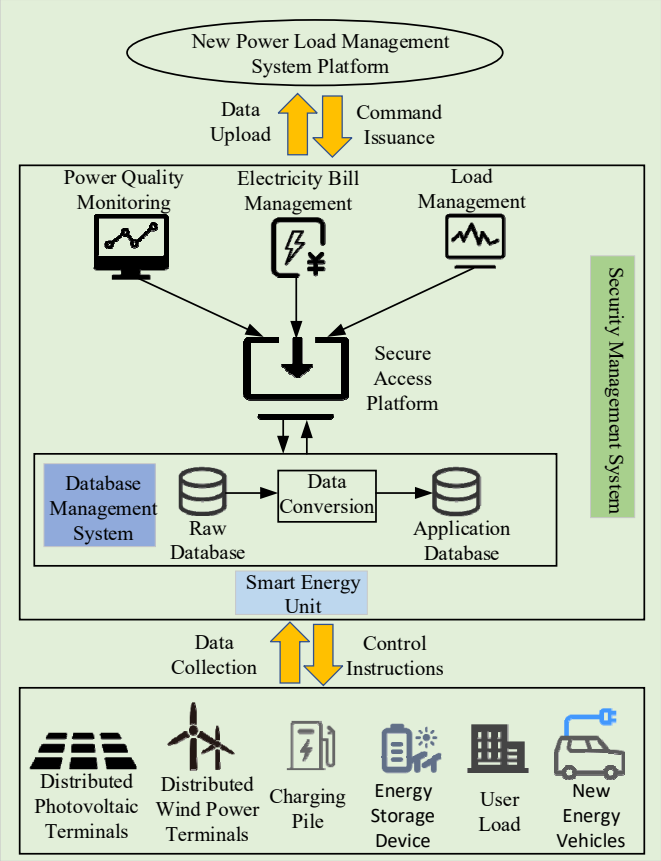

Figure 1. New power load management system.

The main purpose of the buck converter is to convert high-voltage bus voltage to low-voltage bus voltage to meet load requirements. Since buck converters generally have external enclosures for protection, damage or deformation of the enclosure can lead to ground faults. As a result, researchers both domestically and internationally have conducted extensive research on fault detection for DC/DC converters [4–7]. Currently, there are three main methods: analytical models, signal processing, and data-driven methods. Reference [8] introduced a periodic decoupling method in the induction motor model to identify the fault state of switching transistors by detecting the output of stator current and mechanical angular velocity. Reference [9] utilized batch mode regression estimation methods to diagnose parametric faults in the circuit, treating the induction motor model as a periodic decoupling structure to isolate switching transistor faults. Analytical model methods have advantages in precise systems but face significant difficulties in high-order system applications. Reference [10] used Bayesian parameter estimation to integrate current and voltage information from different sensors into multi-feature data from a single sensor output. Reference [11] addressed open-circuit faults in the midpoint-clamped inverter switches by processing DC-side current and employing an adaptive sliding mode observer for fault diagnosis of the inverter. Reference [12] adopted a feature-level fusion approach for fault diagnosis in photovoltaic grid-connected inverters, selecting grid-side currents and bridge arm voltages, and using wavelet transforms for fault processing. Signal processing methods are more widely applicable but still require professional diagnostic experience to interpret new features obtained from processed signals, leading to lower diagnostic efficiency. Reference [13] used fuzzy reasoning to convert complex equipment status information into easily understandable fuzzy sets for fault detection and status observation. Reference [14] established fault trees using the random forest algorithm to achieve fault diagnosis for multi-level converters, improving diagnosis accuracy and speed. Reference [15] employed artificial neural network classification techniques for diagnosing

faults in three-phase four-bridge-arm inverters, precisely extracting harmonic components and switching frequencies from bridge arm voltages as key fault features to enhance fault diagnosis accuracy and efficiency. Data-driven methods do not require exploration of the system's internal working principles, but their data collection and processing steps are relatively complex. The reliability and accuracy of this method largely depend on the analyst's expertise and experience.

However, these methods often have certain limitations in practical applications. Reference [16] uses bond graph as a tool to propose a modeling method for studying the characteristics of high-power rectifier supply systems, creating a complex mathematical model to predict the system's health state. Although this method can achieve high detection accuracy, its model construction process is complex. When there is strong system nonlinearity or many unknown parameters, the computational burden is heavy, making real-time application difficult. Some studies employ wavelet transform, Fourier analysis, and similar techniques for feature extraction and spectral analysis of fault signals [17–19]. While signal processing methods have certain advantages in detecting high-frequency noise and transient faults, detection results often lack stability when fault features are weak or noise levels are high. In recent years, machine-learning-based fault detection methods have gained traction, such as fault classification techniques based on neural networks and support vector machines [20,21]. However, data-driven methods generally require large amounts of training data and have high hardware demands, which increases implementation costs.

To address the above issues, this paper proposes a multi-point common-mode voltage ground fault detection method for a synchronous buck photovoltaic-energy storage DC/DC converter. The main contributions are as follows:

1. The proposed method relies solely on basic voltage measurements, simplifying complexity and making the approach more suitable for practical applications;
2. Through multi-point common-mode voltage measurements combined with filtering and thresholding, the method achieves reliable detection with lower computational cost;
3. This method requires fewer sensors and computational resources, making it cost-effective and especially suited for resource-constrained environments.

By integrating voltage measurements and feature parameter extraction, this method overcomes the low sensitivity and inaccurate fault localization of traditional approaches. The method analyzes the relationship between the common-mode voltage at the midpoint of the bridge arm and the input positive bus voltage, switch voltage, and output positive bus voltage. After filtering out high-frequency components, the average voltage values are obtained. By comparing these, ground fault detection for the synchronous buck DC/DC converter is achieved, determining the precise fault location and analyzing the results. This method requires few inputs, has simple criteria, and is suitable for fault diagnosis in power electronic circuits.

2. Equivalent Model and Ground Fault Analysis of Photovoltaic Storage DC Devices

2.1. Equivalent Model of Buck Converter

The photovoltaic energy storage direct current system is a system that utilizes solar photovoltaic arrays for power generation and achieves energy storage and supply through a storage system. As shown in Figure 2, the system consists of a photovoltaic array, a synchronous rectification buck converter, an energy storage system, and an output load. The photovoltaic array, as the core component of the photovoltaic energy storage system, converts solar energy into electrical energy. This energy is then processed by a synchronous rectification buck converter composed of switches S1 and S2 to reduce the output voltage of the photovoltaic array, thereby meeting the load requirements of the user [22]. The capacitor C_{in} is used to absorb the harmonic current generated by the photovoltaic array. The photovoltaic energy storage system is responsible for storing excess electrical energy and releasing it when the load requires power. The control module of the photovoltaic array monitors the state of the lithium-ion battery and controls its charging and discharging

processes, ensuring the safety and longevity of the battery [23–25]. The control module of the photovoltaic array uses the maximum power point tracking (MPPT) algorithm, which can detect the generated voltage of the solar panels in real-time. By continuously adjusting the operating point of the photovoltaic array, this algorithm maximizes the output power, thereby optimizing the utilization of solar energy. The operational state of the photovoltaic energy storage system mainly depends on the input irradiance. When the irradiance is too low to meet the power demands of the load, the lithium-ion battery discharges, releasing stored energy to supply the load, and the battery's state of charge (SOC) gradually decreases. By adjusting the output power of the photovoltaic array through the control module, the system can maintain optimal operation under varying irradiance conditions, thereby achieving efficient utilization of solar energy. Meanwhile, the charge and discharge processes of the lithium-ion battery are also monitored and regulated by the control module to ensure safe operation and extend the battery's lifespan. The design and control strategy of this photovoltaic energy storage DC system can provide a reliable power supply in practical applications, maximize the utilization of solar energy resources, reduce reliance on traditional energy sources, and achieve sustainable development goals [26].

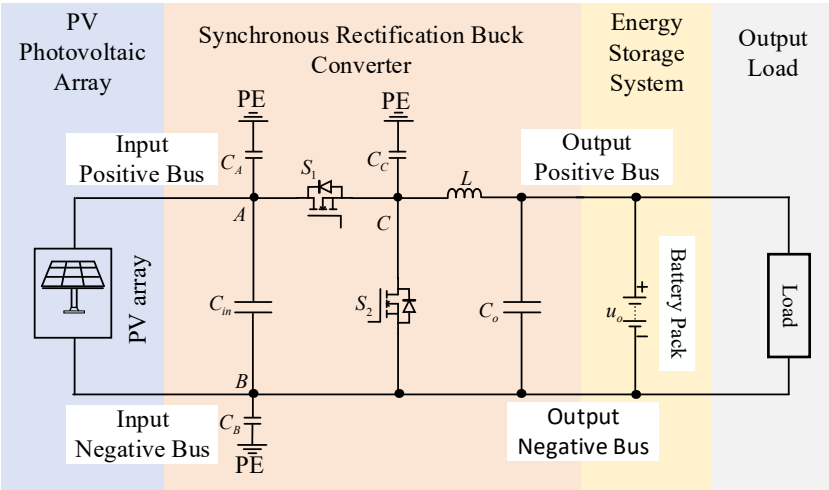

Figure 2. System block diagram of photovoltaic DC/DC converter.

The buck converter has parasitic capacitance between the heatsink and the chassis relative to the protective earth (PE), typically on the order of hundreds of picofarads. This includes the capacitance between the positive bus at point A and ground (C_A), the negative bus at point B and ground (C_B), and the midpoint of the bridge arm at point C and ground (C_C). When the switch S2 is driven by a signal, the voltage across the parasitic capacitance C_C at point C to ground continuously changes. This varying voltage causes the parasitic capacitance C_C to charge and discharge, leading to common-mode voltage.

When analyzing grounding faults in the buck converter, the following assumptions are made to facilitate the analysis of the fault process:

1. The input voltage u_{in} and output voltage u_o remain constant;
2. All components are considered ideal;
3. The input capacitor C_{in} and output capacitor C_o are sufficiently large.

Given the assumption that the input voltage u_{in} and output voltage u_o remain constant, the input voltage u_{in} after photovoltaic generation and the output voltage u_o can be equivalent to voltage sources. During one switching cycle, let the duty cycle of the switch be D, and the average current across the switch S1 is

$$i_{S1} = Di_L \tag{1}$$

The average voltage across the switch S2 is

$$u_{S2} = Du_{in} - (1 - D)u_o \tag{2}$$

The switch S2, which connects point C (where the potential continuously changes) to the negative input bus, is equivalent to a controlled voltage source. By averaging the voltage over one switching cycle during the on/off states of the switch, and by averaging the current through switch S1 over the switching cycle to model it as a controlled current source, the original circuit can be represented by an averaged model over one switching period.

Based on Kirchhoff's voltage law and Ohm's law, after substituting the voltages and currents at the nodes of the buck converter, the equivalent model is shown in Figure 3. In this model, u_{in}, u_{s}, and u_{o} represent the equivalent voltage sources corresponding to the input voltage, switch S2, and output voltage, respectively, while is represents the equivalent current source for switch S1.

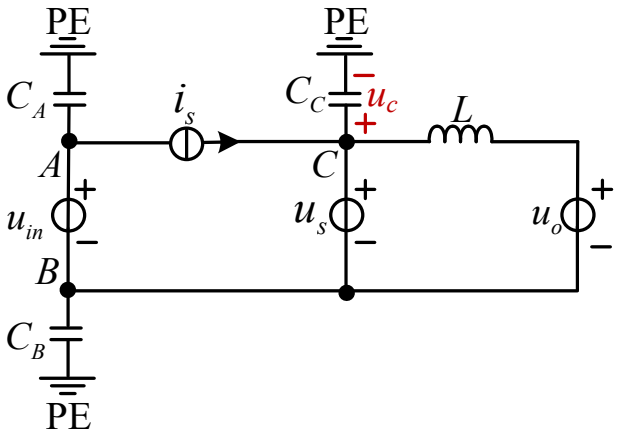

Figure 3. Equivalent model of buck converter under normal operation.

In Figure 3, the voltage sources u_{in}, u_{s}, u_{o}, and the current source i_{s} satisfy Kirchhoff's voltage law and Kirchhoff's current law. Under the influence of independent sources, common-mode noise current flows through the parasitic capacitances between each node and ground, circulating between the converter and the PE.

Using the superposition theorem, we consider the case when only the voltage source u_{in} is active (with other voltage sources short-circuited and current sources open-circuited). At this time, the parasitic capacitances C_{B} and C_{C} are in parallel and form a conductive loop with the voltage source u_{in} and parasitic capacitance C_{A}. According to Kirchhoff's voltage law, the voltage across the parasitic capacitance C_{C} can be expressed as

$$u_c = -\frac{C_A}{C_A + C_B + C_C} u_{in} \tag{3}$$

We also consider the case when only the voltage source u_{s} is active. At this time, the parasitic capacitances C_{A} and C_{B} are in parallel and form a conductive loop with the voltage source u_{s} and parasitic capacitance C_{C}. According to Kirchhoff's voltage law, the voltage across the parasitic capacitance C_{C} can be expressed as

$$u_c = \frac{C_A + C_B}{C_A + C_B + C_C} u_s \tag{4}$$

In a case where the only current source i_{s} is active, the parasitic capacitance C_{C} is connected between the positive terminal of the current source i_{s} and the PE, while parasitic capacitances C_{A} and C_{B} are connected between the negative terminal of the current source i_{s} and the PE. In this case, during the simplification process, u_{in}, u_{s}, and u_{o} are considered

short-circuited, so the parasitic capacitance C_C is short-circuited by the current source i_s, resulting in C_C being connected to the PE on both sides, with its potential being zero.

We consider the case when only the voltage source u_o is active. In this case, the voltage source u_o is short-circuited, which results in the parasitic capacitance C_C being short-circuited on both sides, making its potential zero.

According to the superposition theorem, by summing the effects of each source, the voltage u_{c1} across the parasitic capacitance C_C during normal operation of the buck converter can be expressed as

$$u_{c1} = \frac{C_A + C_B}{C_A + C_B + C_C} u_s - \frac{C_A}{C_A + C_B + C_C} u_{in} \tag{5}$$

2.2. Ground Fault of the Positive Input Bus in the Buck Converter

When a grounding fault occurs at point A on the positive input bus of the buck converter, the corresponding equivalent model is shown in Figure 4. Under the influence of the independent sources, common-mode current flows through the parasitic capacitances between each node and ground, circulating between the converter and PE.

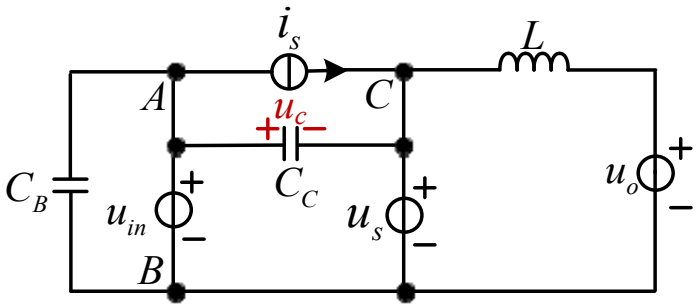

Figure 4. Equivalent model of the positive input bus ground fault in the buck converter.

Using the superposition theorem, we consider the case when only the voltage source u_{in} is active (with other voltage sources short-circuited and current sources open-circuited). At this time, the parasitic capacitances C_B and C_C are in parallel, forming a conductive loop with the voltage source u_{in}. According to Kirchhoff's voltage law, the voltage across the parasitic capacitance C_C can be expressed as

$$u_c = -u_{in} \tag{6}$$

Considering the case when only the voltage source u_s is active, the parasitic capacitance C_C forms a conductive loop with the voltage source u_s. According to Kirchhoff's voltage law, the voltage across the parasitic capacitance C_C can be expressed as

$$u_c = u_s \tag{7}$$

Considering the case when only the current source i_s is active, during the simplification process, u_{in}, u_s, and u_o are considered short-circuited. As a result, the parasitic capacitance C_C is short-circuited by the current source i_s, leading to both sides of the parasitic capacitance C_C being connected, causing its potential to be zero.

We consider the case when only the voltage source u_o is active. Due to the grounding fault at the positive input bus, the parasitic capacitance C_C is short-circuited on both sides, causing its potential to be zero.

According to the superposition theorem, by summing the effects of each source, the voltage u_{c2} across the parasitic capacitance C_C during the grounding fault of the buck converter's positive input bus can be expressed as

$$u_{c2} = u_s - u_{in} \tag{8}$$

2.3. Ground Fault of the Negative Input Bus in the Buck Converter

When a grounding fault occurs at point B on the positive input bus of the buck converter, the corresponding equivalent model is shown in Figure 5. Under the influence of the independent sources, common-mode current flows through the parasitic capacitances between each node and ground, circulating between the converter and the PE.

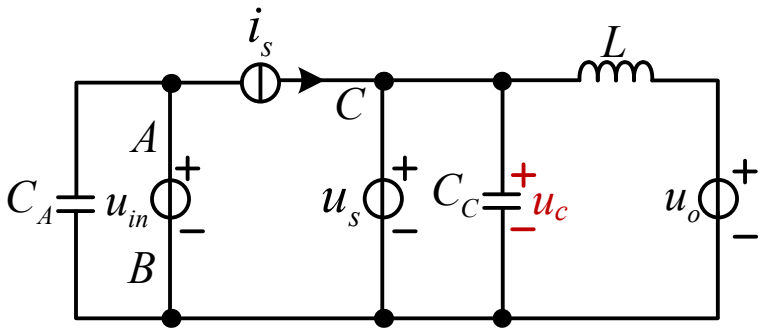

Figure 5. Equivalent model of the negative input bus ground fault in the buck converter.

Using the superposition theorem, when considering only the voltage source u_{in} (with other voltage sources short-circuited and current sources open-circuited), a grounding fault at both ends of C_{C} results in the capacitance being short-circuited, causing the voltage across the parasitic capacitance C_{C} to be zero.

When only the voltage source u_{s} is active, with a grounding fault occurring at the negative input bus, the parasitic capacitance C_{C} forms a conductive loop with the voltage source u_{s}. According to Kirchhoff's voltage law, the voltage across the parasitic capacitance C_{C} can be expressed as

$$u_c = u_s \tag{9}$$

Considering the case when only the current source i_{s} is active, during the simplification process, u_{in}, u_{s}, and u_{o} are considered short-circuited. As a result, the parasitic capacitance C_{C} is short-circuited by the current source i_{s}, leading to both sides of the parasitic capacitance C_{C} being connected, making its potential zero.

When only the voltage source u_{o} is active, a grounding fault occurs at the negative input bus, causing the parasitic capacitance C_{C} to be short-circuited on both sides, making its potential zero.

According to the superposition theorem, by summing the effects of each source, the voltage u_{c3} across the parasitic capacitance C_{C} during a grounding fault of the buck converter's negative input bus can be expressed as

$$u_{c3} = u_s \tag{10}$$

2.4. Ground Fault of the Positive Output Bus in the Buck Converter

When a grounding fault occurs at point C on the positive input bus of the buck converter, the corresponding equivalent model is shown in Figure 6. Under the influence of the independent sources, common-mode current flows through the parasitic capacitances between each node and ground, circulating between the converter and the PE.

Using the superposition theorem, when only the voltage source u_{in} is active (with other voltage sources short-circuited and current sources open-circuited), a grounding fault at the ends of the parasitic capacitance C_{C} results in the capacitance being short-circuited, causing the voltage across C_{C} to be zero.

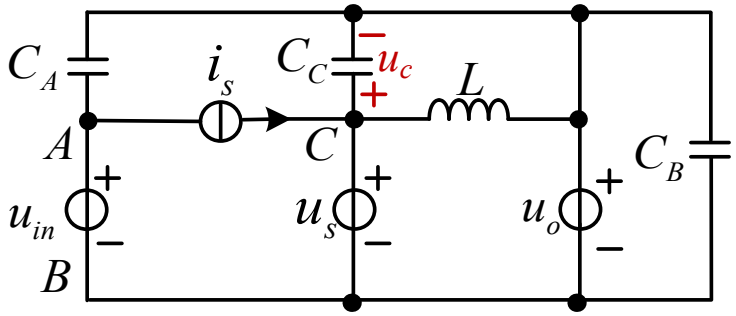

Figure 6. Equivalent model of the positive output bus ground fault in the buck converter.

We consider the case when only the voltage source u_s is active. In this situation, a grounding fault occurs at the positive output bus, and the parasitic capacitance C_C forms a conductive loop with the voltage source u_s. According to Kirchhoff's voltage law, the voltage across the parasitic capacitance C_C can be expressed as

$$u_c = u_s \tag{11}$$

We consider the case when only the current source i_s is active. During the simplification process, u_{in}, u_s, and u_o are considered short-circuited. As a result, the parasitic capacitance C_C is short-circuited by the current source i_s, leading to both sides of C_C being connected and its potential being zero.

We consider the case when only the voltage source u_o is active. In this situation, due to a grounding fault at the positive output bus, the parasitic capacitance C_C forms a conductive loop with the voltage source u_o. According to Kirchhoff's voltage law, the voltage across the parasitic capacitance C_C can be expressed as

$$u_c = -u_o \tag{12}$$

According to the superposition theorem, by summing the effects of each source, the voltage u_{c4} across the parasitic capacitance C_C during a grounding fault at the positive output bus of the buck converter can be expressed as

$$u_{c4} = u_s - u_o \tag{13}$$

3. Ground Fault Detection Method for Photovoltaic DC Devices

Based on the theoretical analysis above, this paper proposes a method for detecting grounding faults in a synchronous buck photovoltaic energy storage DC/DC converter. The method first constructs an equivalent circuit model of the buck converter and then compares the actual sampled state variables with the expected values derived from this model. A grounding fault is detected when the sampled state variables meet predefined fault detection criteria. Finally, a set of precise fault location rules is designed by thoroughly analyzing the fault characteristics under different fault scenarios.

First, voltage signals of the buck converter during operation are collected to diagnose whether a grounding fault exists and its specific location by monitoring the voltage u_c across the parasitic capacitance C_C. Data on u_c, the input voltage u_{in}, switch voltage u_s, and output voltage u_o are also collected.

Next, a low-pass filter is used to extract the switching high-frequency components and obtain their average values, resulting in the average voltage u_{c_avg} across the parasitic capacitance C_C as well as the average values of u_{in}, u_s, and u_o.

Finally, after obtaining the filtered average value of the parasitic capacitor voltage u_{c_avg}, the result is determined by summing it with the input voltage u_{in}, the average value of the switching tube voltage u_{s_avg}, and the output voltage u_o. The grounding fault identification signal is defined as λ. When different fault conditions occur, real-time

monitoring of the fault conditions in the buck converter is performed by detecting different identification signals to determine the fault location. This study sets an error threshold of 10% to ensure the accuracy and reliability of fault identification. The recognition signal λ is categorized into four different cases:

When λ = 1, the buck converter operates normally;

When λ = 2, a grounding fault occurs at the positive input bus;

When λ = 3, a grounding fault occurs at the negative input bus

When λ = 4, a grounding fault occurs at the positive output bus;

Based on the above principles, the variations in the average voltage u_{c_avg} across the parasitic capacitance C_C under different fault scenarios were investigated. By constructing an equivalent model, the mathematical relationships between u_{c_avg} and the input voltage u_{in}, output voltage u_o, and the average switch voltage u_{s_avg} were derived. Further, the four different detection scenarios for u_{c_avg} were classified and identified, matching different voltage signals with the recognition signals to achieve precise fault signal extraction and localization, ensuring the timeliness and accuracy of the detection.

When the buck converter is operating, the detected average value of the parasitic capacitance voltage C_C is u_{c_avg}

$$0.9u_{c1} \leq u_{c\_avg} \leq u_{c1} \tag{14}$$

At this point, the recognition signal λ = 1 indicates that the buck converter is operating normally.

When the buck converter is operating, the detected average value of the parasitic capacitance voltage C_C is u_{c_avg}

$$0.9u_{c2} \leq u_{c\_avg} \leq u_{c2} \tag{15}$$

At this point, the recognition signal λ = 2 indicates a grounding fault at the positive input bus of the buck converter.

When the buck converter is operating, the detected average value of the parasitic capacitance voltage C_C is u_{c_avg}

$$0.9u_{c3} \leq u_{c\_avg} \leq u_{c3} \tag{16}$$

At this point, the recognition signal λ = 3 indicates a grounding fault at the negative input bus of the buck converter.

When the buck converter is operating, the detected average value of the parasitic capacitance voltage C_C is u_{c_avg}

$$0.9u_{c4} \leq u_{c\_avg} \leq u_{c4} \tag{17}$$

At this point, the recognition signal λ = 4 indicates a grounding fault at the positive output bus of the buck converter.

Figure 7 shows the fault diagnosis flowchart for the buck photovoltaic energy storage DC/DC converter. By distinguishing between different recognition signals and comparing the mathematical relationships between the average voltage u_{c_avg} of the parasitic capacitance C_C, the input voltage u_{in}, output voltage u_o, and the average switch voltage u_{s_avg} under four conditions—normal operation, positive input bus grounding fault, negative input bus grounding fault, and positive output bus grounding fault—the effective fault information is extracted. Subsequently, this extracted information is compared and analyzed with data from the actual operation of the buck converter to achieve rapid and accurate fault diagnosis and effectively locate the specific grounding fault.

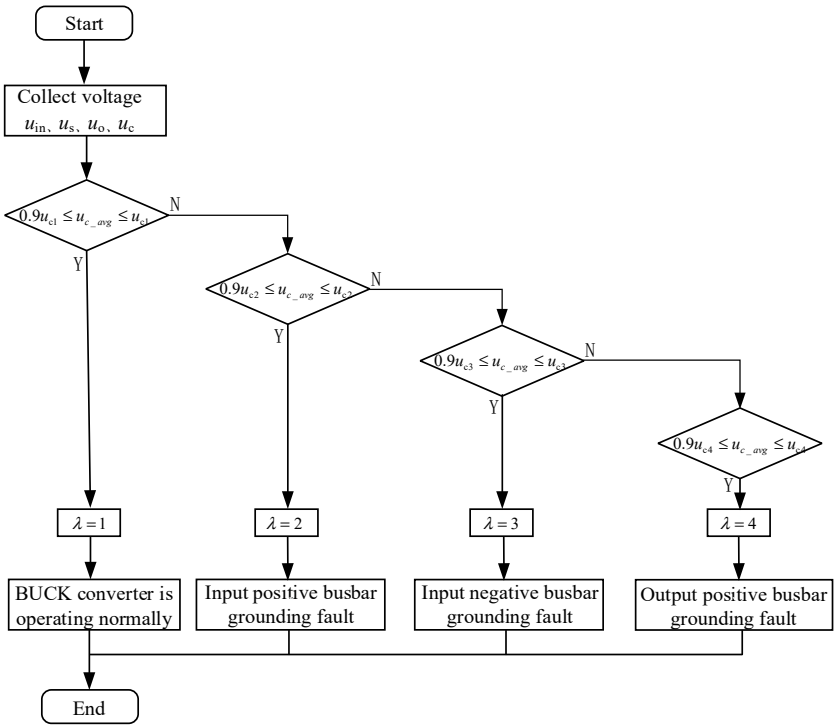

Figure 7. Ground fault detection flowchart for buck converter.

4. Simulation Verification

To verify the accuracy of the theoretical analysis of grounding fault detection for the synchronous buck photovoltaic energy storage DC/DC converter, this study constructed simulation models for three types of grounding faults using the Simulink toolbox in the MATLAB 2022a environment. In the simulation, grounding fault signals were applied to points A, B, and C of the buck converter at 0.05 s. The dynamic changes in the recognition signals and the corresponding average voltage u_{c_avg} of the parasitic capacitance C_C were monitored throughout the process. By observing these changes, it is possible to determine whether a grounding fault has occurred in the synchronous buck photovoltaic energy storage DC/DC converter and further pinpoint the specific location of the fault. The parameters of the simulation model and the relevant parasitic parameters of the components are detailed in Table 1.

Table 1. Simulation model parameters and parasitic parameters.

Variables	Definition	Parameter
u_{in}	Input voltage	35 V
u_o	Output voltage	14 V
C_{in}	Input capacitance	470 μF
L	Excitation inductance	80 μH
C_o	Output capacitor	560 μF
f_s	Switching frequency	40 kHz
C_A	Parasitic capacitance	100 pF
C_B	Parasitic capacitance	100 pF
C_C	Parasitic capacitance	100 pF

As shown in Figure 8, the input voltage u_{in}, output voltage u_o, and the average voltage u_{s_avg} of switch S2 in the photovoltaic energy storage DC/DC converter is represented from top to bottom. During the periodic switching of the transistor, the output voltage and current of the photovoltaic cell are measured in real-time. These measurements are integrated with a closed-loop control system to implement the maximum power point tracking (MPPT) algorithm, which stabilizes the input voltage at approximately 35 V, while

maintaining the output voltage at around 14 V and the average voltage of the switch at about 14 V.

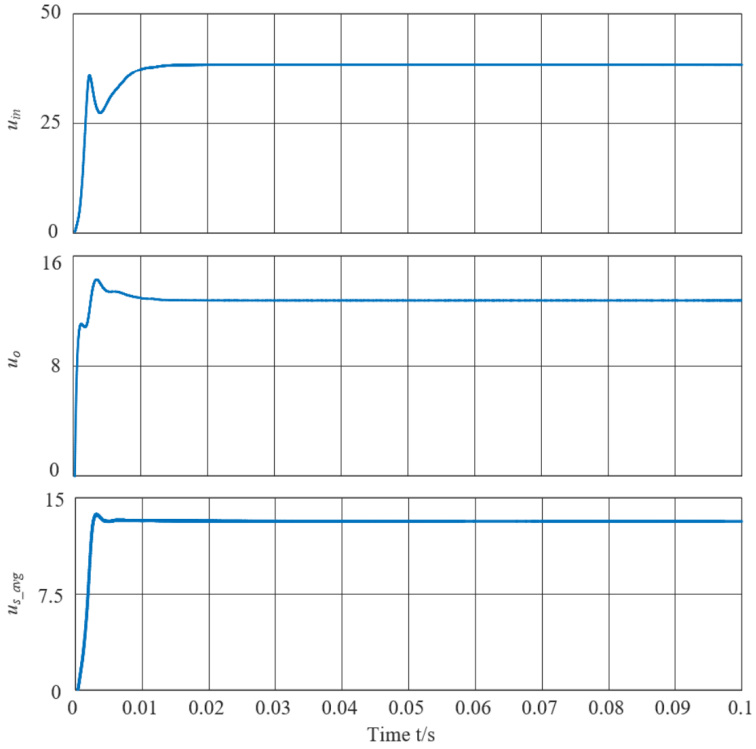

Figure 8. Waveforms of input voltage u_{in}, output voltage u_o, and average voltage u_{s_avg} of switching tube S2 in photovoltaic energy storage DC/DC converter system.

When the photovoltaic energy storage DC/DC converter is operating normally, the waveforms of the recognition signal and the average voltage u_{c_avg} of the parasitic capacitance C_C are shown in Figure 9. Under these conditions, the average voltage of the parasitic capacitance C_C remains stable at −2.4 V. This value aligns with the theoretical average derived from the analysis, confirming that no grounding fault has occurred in the buck converter. Consequently, the identification signal $\lambda = 1$.

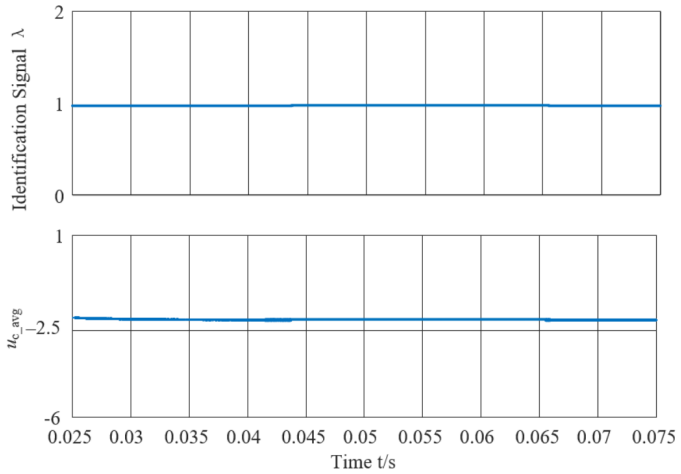

Figure 9. Waveforms of identification signal λ and average voltage u_{c_avg} of parasitic capacitor C_C under normal operation.

At 0.05 s, a grounding fault simulation signal was applied to point A of the input positive bus of the photovoltaic energy storage DC/DC converter. The subsequent changes in the recognition signal λ and the average voltage u_{c_avg} across the parasitic capacitance

C_C are illustrated in Figure 10. Following the grounding fault, the average voltage of the parasitic capacitance C_C experienced a significant drop from its original value of −2.4 V to −21 V, which aligns with the predictions from the theoretical analysis. Additionally, the fault identification signal λ transitioned from state 1 to state 2 within 20ms, confirming that a grounding fault occurred at the input positive bus of the photovoltaic energy storage DC/DC converter.

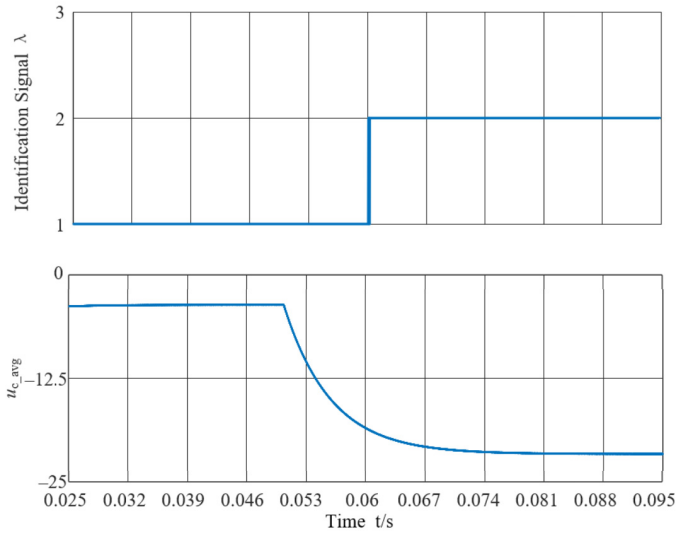

Figure 10. Waveforms of identification signal λ and average voltage u_{c_avg} of parasitic capacitor C_C under input positive bus grounding fault.

At 0.05 s, a grounding fault simulation signal was applied to point B of the input negative bus of the photovoltaic energy storage DC/DC converter. The resulting changes in the identification signal λ and the average voltage u_{c_avg} across the parasitic capacitance C_C are presented in Figure 11. Following the grounding fault occurred, the average voltage of the parasitic capacitance C_C significantly increased, rising from the initial −2.4 V to 14 V, which aligns with the theoretical analysis results. Concurrently, the fault recognition signal λ transitioned from state 1 to state 3 within 20ms, confirming that a grounding fault occurred at the input negative bus of the photovoltaic energy storage DC/DC converter.

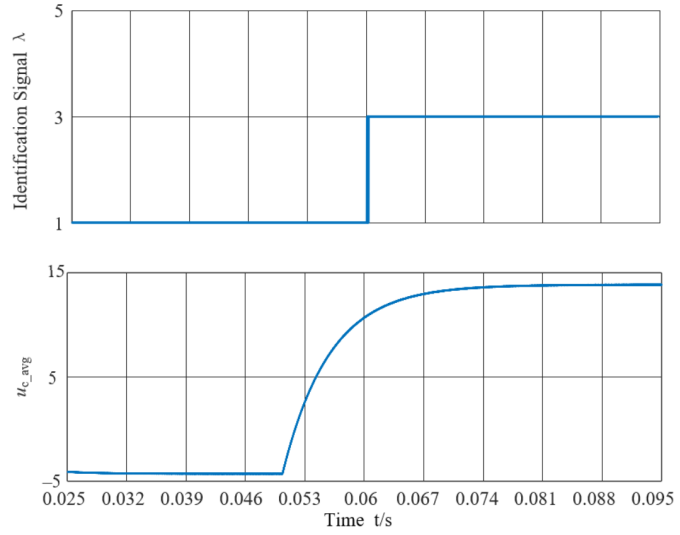

Figure 11. Waveforms of identification signal λ and average voltage u_{c_avg} of parasitic capacitor C_C under input negative bus grounding fault.

At 0.05 s, a grounding fault simulation signal was applied to point C of the output positive bus of the photovoltaic energy storage DC/DC converter. The changes in the

recognition signal λ and the average voltage u_{c_avg} of the parasitic capacitance C_C are shown in Figure 12. After the grounding fault occurred, the average voltage of the parasitic capacitance C_C changed from the initial −2.4 V to 0 V, consistent with the theoretical analysis results. Meanwhile, the fault identification signal λ changed from state 1 to state 4 within 20 ms, confirming that a grounding fault occurred at the output positive bus of the photovoltaic energy storage DC/DC converter.

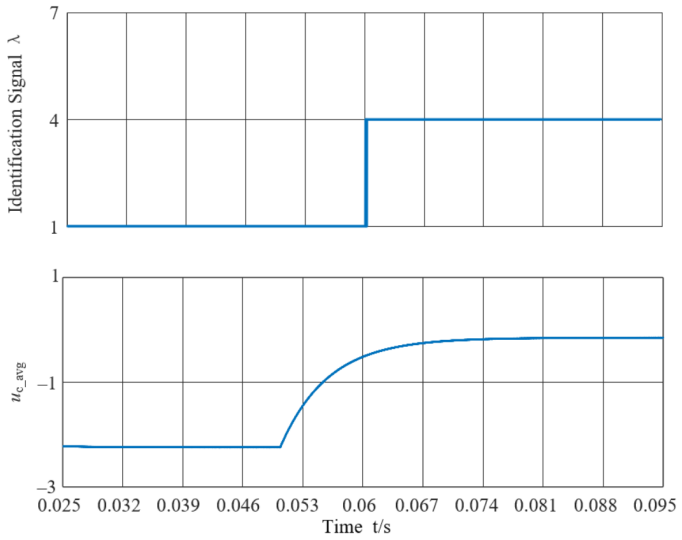

Figure 12. Waveforms of identification signal λ and average voltage u_{c_avg} of parasitic capacitor C_C under output positive bus grounding fault.

Through simulations of four different scenarios, this study effectively demonstrates the reliability of the proposed grounding fault detection method for the synchronous buck photovoltaic energy storage DC/DC converter. This method not only accurately identifies the operational status of the converter during normal operation but also promptly captures fault signals when a grounding fault occurs, enabling timely fault diagnosis. Furthermore, it successfully distinguishes between different fault types: input positive bus grounding fault, input negative bus grounding fault, and output positive bus grounding fault.

5. Experimental Validation

To further validate the effectiveness of the proposed grounding fault detection scheme, an experimental setup was constructed based on the RT-LAB hardware-in-the-loop (HIL) test platform, as depicted in Figure 13. The circuit parameters and controller parameters utilized in the experiment were kept consistent with those in the simulation model to ensure comparability and reliability of the results.

In the experiment, switches were employed to simulate grounding faults artificially. These switches were connected between the input positive bus A and ground, the input negative bus B and ground, and the output positive bus C and ground to create short-circuit grounding conditions. The changes in the parasitic capacitor voltage u_{c_avg} under each fault condition were recorded and compared with the simulation results. By analyzing the differences in voltage waveforms under different fault scenarios, the method's ability to accurately locate the exact position of the grounding fault can be determined.

In the above normal operating state, the maximum power point tracking (MPPT) algorithm is employed to adjust the output of the photovoltaic system in real time, ensuring that it operates at the maximum power point to enhance energy utilization efficiency. By monitoring the output voltage and current of the photovoltaic array, the algorithm can identify the optimal operating point. Subsequently, switch driver signals are applied to control the conduction and cutoff of the switching transistors S1 and S2 in the synchronous buck PV-storage DC/DC converter. The drive signals for switches S1 and S2 are shown in Figures 14 and 15.

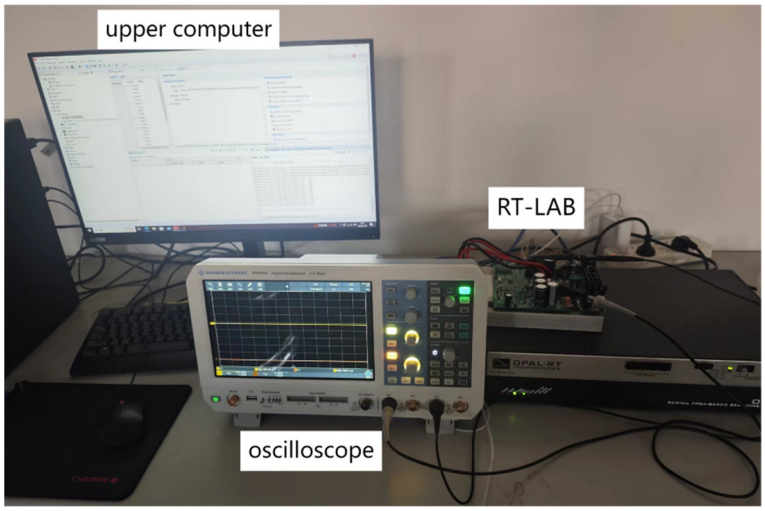

Figure 13. Experimental platform.

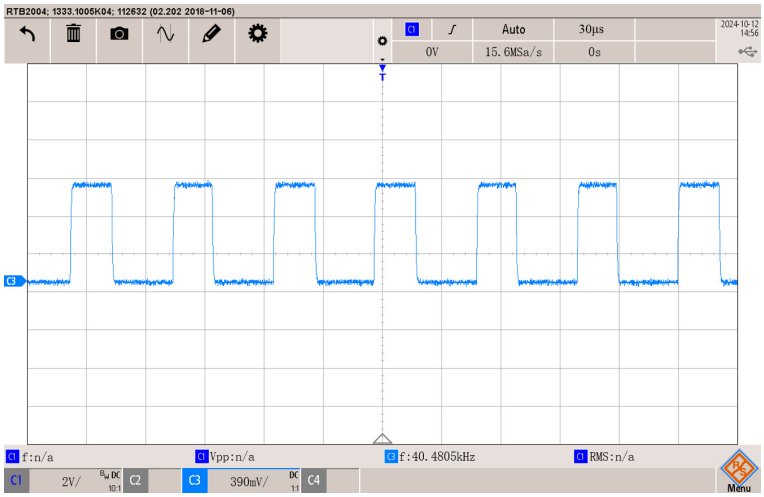

Figure 14. Drive signal for switch S1.

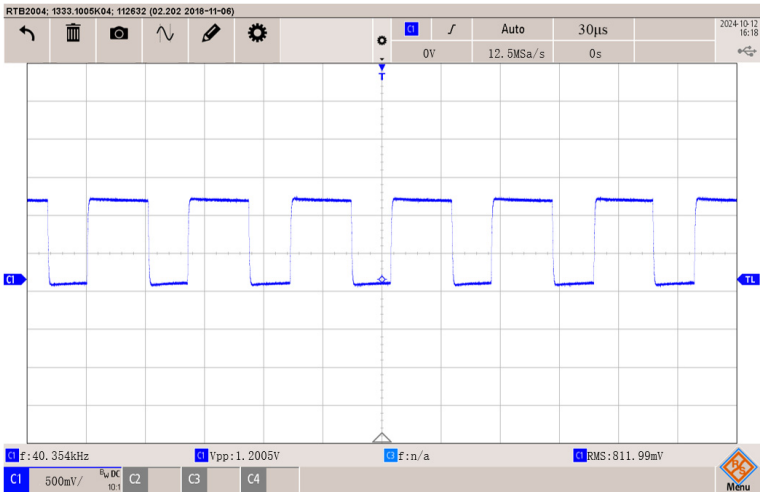

Figure 15. Drive signal for switch S2.

Precise control of the switching transistors is achieved through PWM signals, which are directly influenced by the MPPT algorithm. As solar irradiance and temperature conditions fluctuate, the MPPT algorithm recalculates the optimal operating point and

continuously updates the duty cycle of the PWM signal. This real-time adjustment ensures that the switching devices operate in synchrony with the PV array's maximum power point (MPP), thereby minimizing energy losses and optimizing the performance of the PV-storage system.

As illustrated in Figure 16, during normal operating conditions, the average voltage across the parasitic capacitance C_C, denoted as u_{c_avg}, remains consistently stable at approximately −2.4 V. This steady-state behavior of the parasitic capacitance voltage reflects the expected equilibrium in the system when no faults are present. The stability of u_{c_avg} indicates that the converter is operating within its designed parameters without any significant disturbances.

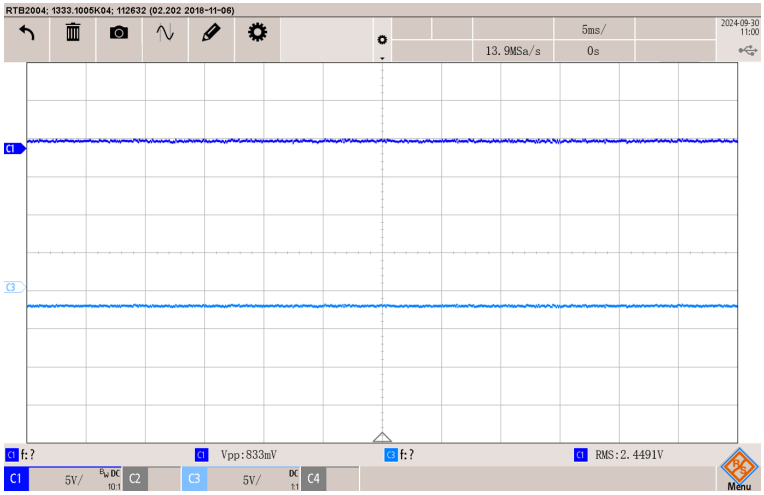

Figure 16. The experimental waveforms of identification signal λ and average voltage u_{c_avg} of parasitic capacitor C_C under normal operation.

Simultaneously, the identification signal λ, derived from monitoring key operational parameters, confirms the proper functioning of the buck converter. This value is designed to serve as a fault detection indicator, remaining within a predefined range that corresponds to normal operation under typical conditions. The λ signal ensures real-time monitoring and provides immediate feedback on the converter's operational status, facilitating prompt detection of any anomalies or faults.

The combination of a stable parasitic capacitance voltage and a nominal identification signal λ verifies that the system is free from any anomalies. These diagnostic metrics serve as reliable indicators that the synchronous buck PV-storage DC/DC converter is efficiently regulating the input and output voltages, maintaining optimal performance in the absence of external or internal faults.

As shown in Figure 17, all voltage signals are within the expected range. When a grounding fault occurs on the input positive bus, the average voltage of the parasitic capacitance C_C drops sharply from −2.4 V to −21 V. This significant change is completed within 20 ms, and the identification signal λ quickly changes from state 1 to state 2, accurately indicating that the fault is located at the input positive bus.

As shown in Figure 18, when a fault signal is applied to the input negative bus, the average voltage of the parasitic capacitance rises from −2.4 V to 14 V. Similarly, within 20 ms, the identification signal λ changes from state 1 to state 3, confirming that a grounding fault has occurred on the input negative bus.

As shown in Figure 19, after applying a grounding fault signal to the output positive bus, the average voltage of the parasitic capacitance significantly changes from the initial −2.4 V to 0 V, and the identification signal λ changes to state 4 within 20 ms, confirming the grounding fault of the output positive bus. The above experimental results demonstrate that the proposed detection method can quickly and accurately identify and locate different

types of grounding faults. The experimental results are consistent with the theoretical analysis, further demonstrating the potential of this method in practical applications.

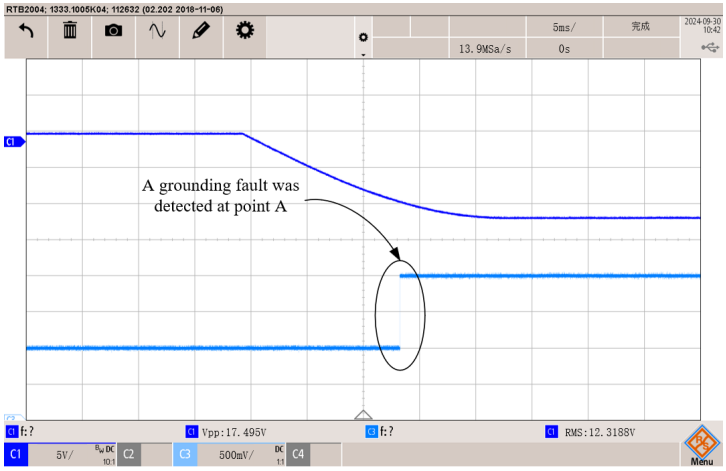

Figure 17. The experimental waveforms of identification signal λ and average voltage u_{c_avg} of parasitic capacitor C_C under input positive bus grounding fault.

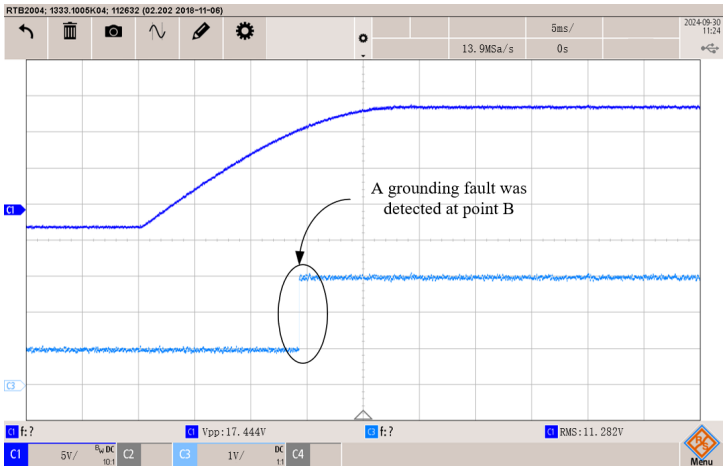

Figure 18. The experimental waveforms of identification signal λ and average voltage u_{c_avg} of parasitic capacitor C_C under input negative bus grounding fault.

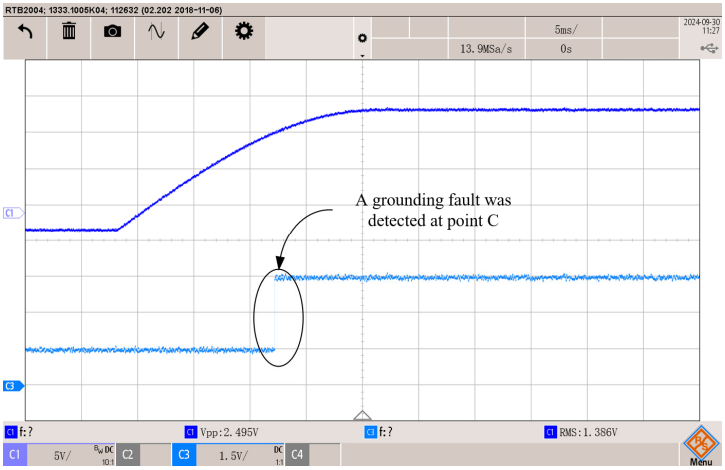

Figure 19. The experimental waveforms of identification signal λ and average voltage u_{c_avg} of parasitic capacitor C_C under output positive bus grounding fault.

6. Conclusions

This paper investigates a ground fault detection method for a synchronous buck DC/DC converter in photovoltaic and storage systems. The method detects the average voltage of the parasitic capacitance at the midpoint of the bridge arm and compares it with the sum of the input voltage, output voltage, and the average switch voltage to determine whether a ground fault has occurred and its specific location. Four scenarios are analyzed in this paper: normal converter operation, input positive bus grounding fault, input negative bus grounding fault, and output positive bus grounding fault. Corresponding equivalent models are established to study the variation of the average parasitic capacitance voltage, enabling effective detection of ground faults in the buck DC/DC converter. Finally, the proposed method's effectiveness and reliability are validated through simulation and experimental verification.

Based on the above simulations and experiments, the following conclusions can be drawn:

1. The proposed method can effectively detect grounding faults in the buck PV-storage DC converter;
2. By analyzing the voltage signal characteristics in different fault scenarios, the accuracy and real-time performance of the detection signal is validated;
3. The applicability of this detection method in practical applications and its potential for optimization are also assessed.

Author Contributions: Investigation, J.Y., J.L., Z.Z. and L.G.; Writing—original draft, K.Z.; Supervision, Z.D. All authors have read and agreed to the published version of the manuscript.

Funding: This research was funded by the Science and Technology Project of State Grid Hebei Electric Power Company, Ltd., grant number SGHEXG00YXJS2310876.

Data Availability Statement: Data is contained within the article.

Conflicts of Interest: Author Kai Zhang was employed by the company State Grid Ningjin Electric Power Supply Company. Jian Yang, Jian Li and Zhongying Zhang were employed by the company State Grid Xingtai Electric Power Supply Company. The remaining authors declare that the research was conducted in the absence of any commercial or financial relationships that could be construed as a potential conflict of interest.

References

1. Xu, M.; Shi, Y.; Xing, J.; Wang, J.; Jin, G.; Liu, Z. Reliability Calculation Method of Microgrid Based on Multi Typical Scene Sampling. *J. Electr. Power Sci. Technol.* **2022**, *37*, 41–49.
2. Zhao, Y.; Zhao, C.; Sun, Z. Research on Grounding Fault Analysis and Grounding Design of DC Microgrid. *Jiangsu Sci. Technol. Inf.* **2022**, *39*, 33–37.
3. Burin, Y.; Suwat, S.; Damien, G.; Hinaje, M.; Phattanasak, M.; Kaewmanee, W.; Vitale, G. Open-Circuit Switch Fault Diagnosis and Accommodation of a Three-Level Interleaved Buck Converter for Electrolyzer Applications. *Electronics* **2023**, *12*, 1349. [CrossRef]
4. Mao, Y.; Yang, L.; Yan, L.; Cui, G. Detection Method of Incipient Inter-Turn Short Circuit Fault of PMSM Based on VMD. *Electr. Mach. Control Appl.* **2022**, *49*, 66–74.
5. Lu, B.; Sharma, S.K. A Literature Review of IGBT Fault Diagnostic and Protection Methods for Power Inverters. *IEEE Trans. Ind. Appl.* **2009**, *45*, 1770–1777.
6. Liao, L.; Gao, H.; He, Y.; Xu, X.; Lin, Z.; Chen, Y.; You, F. Fault Diagnosis of Capacitance Aging in DC Link Capacitors of Voltage Source Inverters Using Evidence Reasoning Rule. *Math. Probl. Eng.* **2020**, *2020*, 1–12. [CrossRef]
7. Guo, Y.; Wang, A.; Yao, X. Fault Diagnosis of Asynchronous Motors Based on BP Neural Network and Wavelet Packet Energy Analysis. *Electr. Mach. Control Appl.* **2022**, *49*, 53–59.
8. Campos-Delgado, U.D.; Espinoza-Trejo, R.D. An Observer-Based Diagnosis Scheme for Single and Simultaneous Open-Switch Faults in Induction Motor Drives. *IEEE Trans. Ind. Electron.* **2011**, *58*, 671–679. [CrossRef]
9. Yue, K.; Liu, Y.; Zhao, P.; Wang, B.; Fu, M.; Wang, H. Dynamic State Estimation Enabled Health Indicator for Parametric Fault Detection in Switching Power Converters. *IEEE Access* **2021**, *9*, 33224–33234. [CrossRef]
10. Zhang, G.; Gao, F.; Shi, Y.; Gao, Y. Multi-Feature Fusion Diagnosis Method of Open-Circuit Fault for Traction Inverter Based on Bayesian Network. *J. Railw. Sci. Eng.* **2020**, *17*, 732–740.
11. Xu, S.; Huang, W.; He, Y.; Hu, Y.; Cheng, T. Open-Circuit Fault Diagnosis of Neutral Point Clamped Three-Level Grid-Connected Inverter Based on Adaptive Sliding Mode Observer. *Trans. China Electrotech. Soc.* **2023**, *38*, 1010–1022.

12. Min, Y.; Wang, H.; Han, W. Fault Diagnosis of Photovoltaic Grid Inverter Based on Information Fusion. *Electr. Meas. Instrum.* **2014**, *51*, 17–21.
13. Zhang, H.; Ren, J.; Zhong, Y.; Chen, J. Fault diagnosis of power electronics in renewable energy equipment based on fuzzy expert system. In Proceedings of the IEEE International Electric Machines and Drives Conference (IEMDC), Antalya, Turkey, 3–5 May 2007; pp. 864–867.
14. Yang, H.; Xing, W.; Chen, C.; Zhang, W.; Li, C.; Xiang, X.; Li, W. A Fault Detection and Location Strategy for Sub-Module Open-Circuit Fault in Modular Multilevel Converters Based on Random Forest Binary Classifier. *Proc. China Electrotech. Soc.* **2023**, *43*, 3916–3928.
15. Zhao, H.; Xu, H.; Mei, Z.; Cao, Y. Fault Diagnostic System for Inverter Open-Circuit Fault Based on Neural Networks. *Power Electron. Technol.* **2021**, *55*, 45–49.
16. Li, S. Bond Graph Model and Fault Diagnosis Method of High-Power Rectifier Power Supply System. Master's Thesis, Hunan University of Science and Technology, Xiangtan, China, 2012.
17. Yang, Z.; Wu, Z.; Li, H. Invester Fault Diagnose Based on Detecting DC Side Current. *Zhongguo Dianji Gongcheng Xuebao* **2008**, *28*, 18–22.
18. Shen, Y.; Zhou, W.; Ji, Z.; Pan, T. Fault Identification of Converters in Wind Power Generation Systems Based on Wavelet Packet Analysis. *Power Syst. Technol.* **2013**, *37*, 2011–2017.
19. Awadallah, M.A.; Morcos, M.M. Automatic diagnosis andlocation of open-switch fault in brushless DC motor drivesusing wavelets and neuro-fuzzy systems. *IEEE Trans. Energy Convers.* **2003**, *21*, 104–111. [CrossRef]
20. Khomfoi, S.; Tolbert, L.M. Fault diagnosis system for multilevel inverters using a principal component neural network. In Proceedings of the IEEE Power Electronic Specialists Conference, Jeju, Republic of Korea, 18–22 June 2006; pp. 3121–3127.
21. Khomfoi, S. Fault diagnosis and reconfiguration for multilevel inverter drive using AI-based techniques. *IEEE Trans. Ind. Electron.* **2007**, *54*, 2954–2968. [CrossRef]
22. Tian, F.; Li, X.; Gan, Y.; Zhang, G. Analysis on Economic Operation and Energy Storage Allocation of High Proportion New Energy System. *Northeast Electr. Power Technol.* **2023**, *44*, 36–39+44.
23. Mei, S.; Tan, Q.; Dai, M. Energy Storage Capacity Configuration Considering Seasonal Fluctuations of Wind and Photovoltaic Output. *Electr. Power Eng. Technol.* **2022**, *41*, 51–57.
24. Qiu, C.; Ying, Z.; Feng, Y.; Yan, J. Optimal Operation of Hybrid Energy Storage Integrated Micro-Energy Network Considering Carbon Quote. *Electr. Power Eng. Technol.* **2022**, *41*, 119–127.
25. Wang, L.; Chen, Q.; He, G.; Wu, L.; Xia, X. Optimization of Generation Scheduling Considering Battery Energy Storage Life Model. *Power Syst. Autom.* **2019**, *43*, 93–100. [CrossRef]
26. Lu, Z.; Lin, Y.; Qiao, Y.; Wu, L.; Xia, X. Flexibility Supply-Demand Balance in Power System with Ultra-High Proportion of Renewable Energy. *Power Syst. Autom.* **2022**, *46*, 3–16.